Statistical analysis of multipath clustering in an indoor office environment

Emmeric Tanghe, Wout Joseph, M. Lienard, Abdelmottaleb Nasr, Paul Christian Stefanut, Luc Martens, Pierre Degauque

Hindawi Publishing Corporation
EURASIP Journal on Wireless Communications and Networking
Volume 2011, Article ID 263134, 16 pages
doi:10.1155/2011/263134

Research Article

Statistical Analysis of Multipath Clustering in an Indoor Office Environment

Emmeric Tanghe,[1] Wout Joseph,[1,2] Martine Liénard,[2] Abdelmottaleb Nasr,[2] Paul Stefanut,[2] Luc Martens,[1] and Pierre Degauque[2]

[1] *Department of Information Technology, Ghent University-IBBT, Gaston Crommenlaan 8 box 201, 9050 Ghent, Belgium*
[2] *Group TELICE, IEMN, University of Lille, Building P3, 59655 Villeneuve d'Ascq, France*

Correspondence should be addressed to Emmeric Tanghe, emmeric.tanghe@intec.ugent.be

Received 12 August 2010; Revised 15 December 2010; Accepted 21 February 2011

Academic Editor: Nicolai Czink

A parametric directional-based MIMO channel model is presented which takes multipath clustering into account. The directional propagation path parameters include azimuth of arrival (AoA), azimuth of departure (AoD), delay, and power. MIMO measurements are carried out in an indoor office environment using the virtual antenna array method with a vector network analyzer. Propagation paths are extracted using a joint 5D ESPRIT algorithm and are automatically clustered with the K-power-means algorithm. This work focuses on the statistical treatment of the propagation parameters within individual clusters (*intracluster* statistics) and the change in these parameters from one cluster to another (*intercluster* statistics). Motivated choices for the statistical distributions of the intracluster and intercluster parameters are made. To validate these choices, the parameters' goodness of fit to the proposed distributions is verified using a number of powerful statistical hypothesis tests. Additionally, parameter correlations are calculated and tested for their significance. Building on the concept of multipath clusters, this paper also provides a new notation of the MIMO channel matrix (named *FActorization into a BLock-diagonal Expression or FABLE*) which more visibly shows the clustered nature of propagation paths.

1. Introduction

To meet the ever-increasing requirements for reliable communication with high throughput, novel wireless technologies have to be considered. A promising approach to increase wireless capacity is to exploit the spatial structure of wireless channels through multiple-input multiple-output (MIMO) techniques. High-throughput MIMO specifications are already being included in wireless standards, most notably IEEE 802.11n [1], IEEE 802.16e [2], and 3GPP Long-Term Evolution (LTE) [3]. MIMO is one of the principal technologies that will be used by 4G communication networks.

The potential benefits of implementing MIMO are highly dependent on the characteristics of the propagation environment. A lot of progress has been made in the development of different types of MIMO channel models for signal processing algorithm testing [4]. In recent years, the geometry-based stochastic type of channel models, first proposed in [5], gains research interest. These kind of models present a statistical distribution for the propagation path parameters (e.g., direction of arrival, direction of departure, delay, etc.), while also taking some geometry parameters of the environment into account (e.g., the location of scatterers). For the moment, most geometry-based stochastic channel models use propagation path clusters in their description. Clustering of propagation paths seems to occur naturally in wave propagation and as an added benefit helps to reduce the number of statistical parameters needed to construct the model. Examples of geometry-based stochastic channel models can be found in [6–9].

This work investigates the statistics of propagation path parameters including directions of arrival and departure, delay, and power in an indoor office environment. For this,

MIMO channel sounding measurements with a virtual antenna array are carried out on an office floor. Propagation path parameters are extracted from measurement data and are subsequently grouped into clusters using an automatic clustering algorithm. Following, propagation path parameters are split up into an *intercluster* part and an *intracluster* part; the former is representative for the location in propagation path parameter space of the cluster to which the path belongs, while the latter is defined as the propagation path parameter's deviation from the intercluster part. Additionally, a new notational improvement of the wireless channel matrix is proposed which makes the separation of propagation path parameters into intercluster and intracluster parts more visible. This decomposition of the MIMO channel matrix is named *FActorization into a BLock-diagonal Expression (FABLE)*, because the decomposition includes a block-diagonal form of the intracluster parameters.

Next, the intercluster and intracluster dynamics are modelled statistically. Choices for the statistical distributions are physically and statistically motivated; those types of distributions are chosen which in our opinion most accurately agree with the underlying propagation physics and which match the support of the propagation parameters (e.g., the von Mises distribution for angular data). Distributional choices are justified compared to choices made in literature, for example, the stochastic channel models in [6–9]. The main emphasis of this paper is on the good statistical treatment of the data; the soundness of using specific distributions is validated through statistical hypothesis tests. Care is taken in the choice of appropriate hypothesis tests that have sufficient power even at low sample sizes. Additionally, parameter correlations are calculated and tested for their significance. For this, a rank correlation coefficient is used. In our opinion, these kind of tests can be valuable in deciding which parameter correlations can be neglected to reduce model complexity.

The outline of this paper is as follows. First, the MIMO measurements and measurement data processing are detailed in Section 2. Section 3 presents the FABLE construction of the wireless channel transfer function. The correlations and statistical distributions of the propagation path parameters within clusters are discussed in Section 4. The statistical descriptions of the intracluster and intercluster parameters are further discussed in Section 5. Finally, a summary of the work is provided in Section 6.

2. Measurements and Data Processing

2.1. Measurement Setup. The measurement setup for the MIMO measurements is shown in Figure 1 and is detailed in the following along with the measurement procedure. A network analyzer (Agilent E8257D) is used to measure the complex channel frequency response for a set of transmitting and receiving antenna positions. The channel is probed in a 40 MHz measurement bandwidth from 3460 MHz to 3500 MHz. As transmitting (Tx) and receiving antenna (Rx), broadband omnidirectional discone antennas of type Electro-Metrics EM-6116 are used. These antennas can operate in a range from 2 to 10 GHz with a nominal gain of 1 dBi. The gain variation in the measured frequency range is less than 0.5 dB, which shows a sufficiently flat antenna frequency response. The vertical half-power beamwidth of the antenna is 60°. To be able to perform measurements for large Tx-Rx separations, one port of the network analyzer is connected to the Tx through an RF/optical link with an optical fiber of length 500 m. The RF signal sent into the Tx is amplified using an amplifier of type Nextec-RF NB00383 with an average gain of 37 dB. The amplifier assures that the signal-to-noise ratio at the receiving port of the network analyser is at least 20 dB for each measured location of the Tx and Rx. The calibration of the network analyzer is done at the connectors of the Tx and Rx antenna and as such includes both the RF/optical link and the amplifier.

Measurements are performed using a virtual MIMO array [10]. The virtual array is created by moving the antennas to predefined positions along rails in two directions in the horizontal plane. The polarization of both Tx and Rx is vertical for all measurements. For this, stepper motors with a spatial resolution of 0.5 mm are used. Both Tx and Rx are moved along 10 by 4 virtual uniform rectangular arrays (URAs) and are positioned at a height of 1.80 m during measurements (Figure 1). Both antennas were used at the same height of 1.80 m because of practical considerations with the usage of the measurement system, most importantly to keep the antennas far enough away from the rails of the positioning system as possible while also avoiding vibrations of the antennas. The URA elements are spaced 4.29 cm apart, which corresponds to half a wavelength at the highest measurement frequency of 3.5 GHz and ascertains that spatial aliasing does not occur when estimating the directional characteristics of propagation paths [11]. The stepper motor controllers, as well as the network analyzer, are controlled by a personal computer (PC).

One important drawback of using a virtual array is that the surroundings have to remain stationary during the measurement. To assure this, measurements are done at night in the absence of (people) movement. Furthermore, one measurement location was done per night with fluorescent lights switched on only in the hallway. We therefore only expect a few paths impinging on switched-on lights which would not be stationary [12]. At each of 1600 ($10\times4\times10\times4$) combinations of Tx and Rx positioning along the URAs, the network analyser measured the S_{21} scattering parameter ten times (i.e., 10 time observations). The total measurement time for a single MIMO measurement is about 1 h 30 min.

2.2. Measurement Environment. MIMO measurements are carried out on the first floor of an office building. The office floor has a rectangular shape with dimensions 57.9 m by 14.2 m. Figure 2 presents a floor plan of the measurement environment, along with some relevant dimensions. The office floor consists of a hallway, which stretches horizontally in the center of Figure 2 and leads to various offices at the top and bottom in the figure. All inner walls are plasterboard, except for the concrete walls between rooms 118 and 120, and between rooms 115 and 117. Figure 2 also shows locations of the Tx and Rx during measurements. A total of 9 MIMO measurements are performed; their Tx and Rx locations

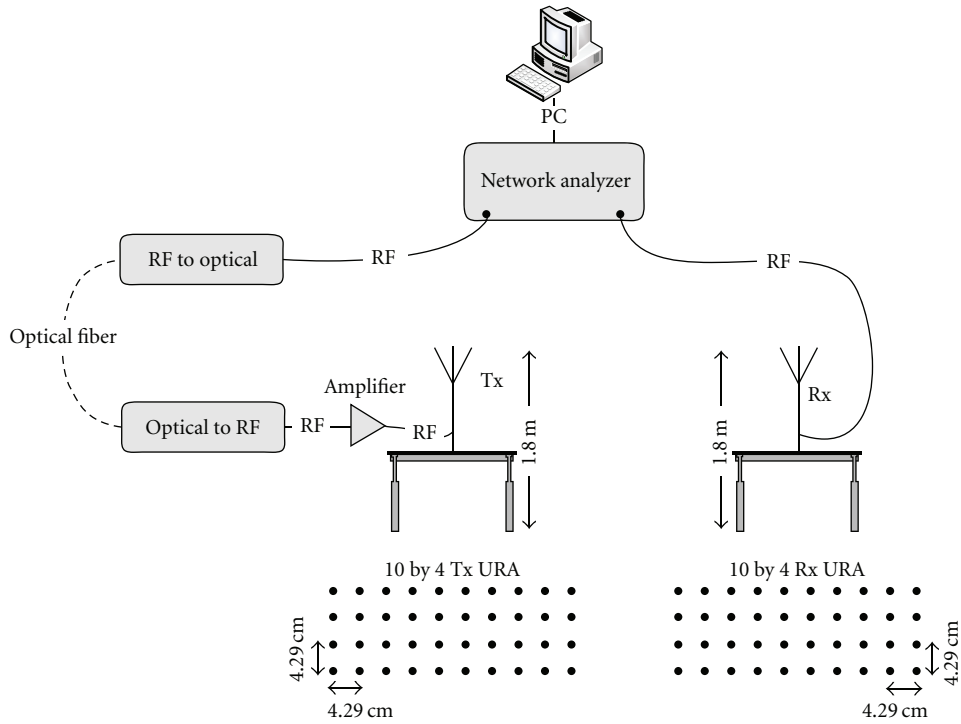

Figure 1: Measurement setup.

are indicated by couples of Tx_i and Rx_i ($i = 1, \ldots, 9$). Measurements are executed in both line-of-sight (LoS) and non-line-of-sight (nLoS) conditions and cover distances between Tx and Rx from 13 to 45 m. Measurement locations 1, 5, and 6 are LoS. Measurements were performed with the doors of the offices closed. The measurement points were selected to make the propagation conditions as diverse as possible in this environment; they include hallway-to-hallway, hallway-to-room, and room-to-room propagation. Additionally, the Tx-Rx line sometimes intersects with only plasterboard walls and sometimes with both plasterboard and concrete walls.

Figure 3(a) shows a picture of the hallway together with the receiving virtual array. The hallway is free of any furniture or clutter otherwise. Figure 3(b) shows a typical office on this floor together with the transmitting virtual array. The offices contain clutter comprising (wood and metal) desks, chairs, desktop PCs, and (metal) filing cabinets.

2.3. Parameter Extraction and Clustering

2.3.1. Extraction of Directional and Delay Properties of Propagation Paths. The directional azimuth of arrival (AoA) and azimuth of departure (AoD) parameters and the delay parameter of propagation paths or multipath components (MPCs) are extracted from measurement data using a 5D unitary ESPRIT (estimation of signal parameters via rotational invariance techniques) algorithm [13]. The ESPRIT algorithm is referred to as 5D, because elevations of arrival and departure are also incorporated in its data model; this alleviates the issue of biased azimuthal angle estimates when only the azimuthal cut is present in the data model [14, 15]. Statistics of the elevation angles are however left out from further analysis in this paper, as these angles possess the "above-below" ambiguity inherent to URAs. The ESPRIT algorithm is used in combination with the simultaneous Schur decomposition procedure for automatic pairing of AoA, AoD, and delay estimates [16]. The coordinate system with respect to which AoA and AoD are defined is shown in Figure 2.

URAs allow easy application of the spatial smoothing technique to increase the number of observations while at the same time increase the detection possibilities of coherent or correlated MPCs [17]. A downside to the technique is the reduced estimation accuracy when the dimensions of the URA subarrays are chosen too small. A possible compromise chooses sub-URAs with dimensions 2/3 of the length in each direction of the original 10 by 4 URA (rounded to the nearest integer), that is, 7 by 3 sub-URAs [18]. In total at both link ends, 64 different 7 by 3 sub-URAs can be found, thereby increasing the number of observations by a factor of 64. Together with the previously mentioned 10 time observations (Section 2.1), the total number of available observations is 640. Furthermore, in the 40 MHz measurement bandwidth, 10 equally spaced frequency points are used with the ESPRIT algorithm. Summarizing, 5D unitary ESPRIT is applied to a 5D vector space of size $7 \times 3 \times 7 \times 3 \times 10$ (spatial dimensions of size 7 and 3 following from each the Tx and Rx URA, and the frequency dimension of size 10) with 640 observations.

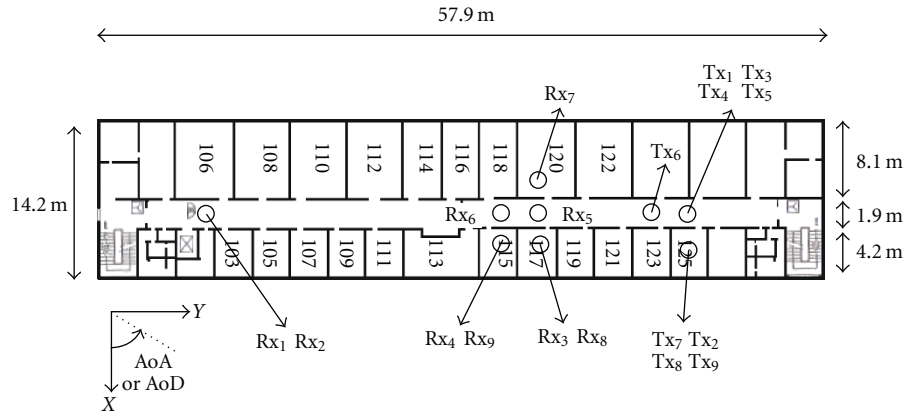

Figure 2: Floor plan of the measurement environment with Tx and Rx locations.

(a) Hallway + Rx (b) Office + Tx

Figure 3: Photos of the measurement environment including the virtual arrays.

The ESPRIT algorithm is used to estimate the 100 most strongest paths from measurement data [9, 19]. Next, the estimated MPCs are postprocessed in the delay domain by considering the power delay profile (PDP, i.e., MPC power versus delay). For a typical PDP, power is concentrated at small delays while at large delays only the noise floor remains. In our measurements, the noise floor is set to the power of the MPC with the largest delay. Following, all MPCs with power less than the noise floor plus a noise threshold of 6 dB are omitted from further analysis [9]. For all measurement locations after postprocessing, between 35 and 87 MPCs are retained. Figure 4(a) shows an AoA/AoD/delay scatter plot of MPCs detected at measurement location 1. The power on a dB scale of each MPC is indicated by a color.

2.3.2. Clustering of Propagation Paths. For our data, automatic joint clustering of AoA, AoD, and delay is performed using the statistical K-power-means algorithm [20]. The K-power-means algorithm result is in agreement with the COST 273 definition of a cluster as a set of MPCs with similar propagation characteristics [8]. Because some parameters for clustering are circular, multipath component distance (MCD) is used as the distance measure for clustering [21]. A delay scaling factor of 5 was used with the MCD, the same value as used for clustering in indoor office environments in [9].

For each measurement location, the number of clusters for the K-power-means algorithm is varied between 2 and 10. The optimal number of clusters is selected according to the Kim-Parks index [22]. The Kim-Parks index is preferred over other more common validity indices that make use of intracluster and intercluster separation measures, such as the Davies-Bouldin and Caliñski-Harabasz indices, as these indices tend to decrease or increase monotonically with the number of clusters [23]. The Kim-Parks index circumvents this behavior by normalizing the index by the index values at the minimum and maximum number of clusters. The Kim-Parks index is, for example, also used for MPC clustering in [19]. The number of detected clusters varies from 3 to 8 between measurement locations, and for all MIMO measurements combined, a total of 45 clusters are found (16 clusters from LoS and 29 clusters from nLoS measurements). Next, to ease the statistical analysis, clearly outlying MPCs are removed from each cluster using the shapeprune algorithm detailed in [20]. To preserve the cluster's original power and shape, outliers are discarded with the restraint that the total

cluster power and the cluster rms AoA, AoD, and delay spreads remain within 10% of their values prior to outlier removal.

After pruning outliers, the average cluster rms AoA and AoD spreads amount to 22° and 36°, respectively. For comparison, cluster rms azimuthal spreads between 2° and 9° were found in [24]. The main reason for the larger spread values obtained here is that the clustering for our measurements takes the delay domain into account, while the study in [24] restricts clustering to the AoA/AoD domains. It is also mentioned in their work that restricting clustering to the azimuthal domains results in more clusters and hence smaller spread values. The spread values obtained here compare more to those in the related work of [24], where values between 22° and 27° are found. Next, cluster rms delay spreads vary between 0.5 and 3.4 ns for LoS. For nLoS, cluster rms delay spreads are between 0.4 and 9.9 ns and are comparable to spreads between 2 and 15 ns found in [19]. Furthermore, the physical realism of clusters was verified by visually cross-referencing cluster mean angles and mean delay (mean propagation distance) with the floor plan in Figure 2. This verification procedure is similar to the one applied in [25], although in this work the procedure is automated with a ray tracer.

Figure 4(b) shows a scatter plot of the clustering result for measurement location 1. For this measurement, the Kim-Parks index estimated the number of clusters at 7. MPCs grouped into different clusters are shown with different marker shapes and colors.

2.4. Limitations of the Measurement Methodology. This section lists the limitations of the MPC measurement methodology. These arise from restrictions of the measurement system in Section 2.1 and could be possible sources of errors in the discussion of the clustered MPC results in Sections 4 and 5.

(i) A full polarimetric antenna radiation pattern is not available for calibration. As such, MPC results presented here include nonchannel antenna effects.

(ii) MPC results are only available for vertical (Tx) to vertical (Rx) polarization. Horizontal polarization is thus missing. Additionally, because a full polarimetric antenna model is lacking, it is not known if the measurement antennas' cross-polarization discrimination is large enough to sufficiently limit power leakage from the horizontal to the vertical polarization.

(iii) Unambiguous results for the MPC elevation parameter are not available due to the use of planar antenna arrays. The missing elevation parameter will affect clustering results; inclusion of an extra parameter will often result in smaller clusters because of the extra dimension in which MPCs can be discriminated.

3. Model

3.1. Signal Model. For the analysis of the intracluster and intercluster propagation path parameters, we use the following basic signal model, based on the double-directional channel model first proposed in [26]. Contrary to the double-directional model, the basic signal model described here includes the Tx and Rx antenna radiation patterns as part of the channel.

For one of the measurement locations, the complex received envelope $h(\phi^A, \phi^D, \tau)$ is written as function of the propagation path parameters: ϕ^A denotes the AoA, ϕ^D is the AoD, and τ is the path delay. The use of MPC clusters is reflected in the complex envelope's notation

$$h\left(\phi^A, \phi^D, \tau\right) = \sum_{c=1}^{n_C} \sum_{k=1}^{n_{P,c}} A_{c,k} \cdot \delta\left(\phi^A - \Phi_{c,k}^A\right) \times \delta\left(\phi^D - \Phi_{c,k}^D\right) \delta(\tau - T_{c,k}). \tag{1}$$

In (1), n_C is the number of clusters and $n_{P,c}$ is the number of MPCs within cluster c. For the kth propagation path in cluster c, $A_{c,k}$ is its received complex amplitude, $\Phi_{c,k}^A$ and $\Phi_{c,k}^D$ are its AoA and AoD, respectively, and $T_{c,k}$ is its delay. $\delta(\cdot)$ denotes the Dirac delta function. We also define $P_{c,k}$ as the power of path k in cluster c, that is, $P_{c,k} = \mathrm{E}[|A_{c,k}|^2]$ where the expectation operator $\mathrm{E}[\cdot]$ is taken over all 640 time observations. Instead of directly modelling the statistics of the complex amplitude $A_{c,k}$, the path's power $P_{c,k}$ will be modelled. To allow statistical analysis of propagation parameters of all measurement locations collectively, the dependence of power $P_{c,k}$ and delay $T_{c,k}$ on distance is removed. Power is rescaled such that the total received MPC power equals one, and the origin of the delay axis is set to coincide with the first arriving MPC. Assuming larger values of c or k mean later arriving paths

$$\sum_{c=1}^{n_C} \sum_{k=1}^{n_{P,c}} P_{c,k} = 1, \qquad T_{1,1} = 0\,\mathrm{ns}. \tag{2}$$

We propose to extend the signal model in (1) by splitting up each of the propagation path parameters into an intercluster and an intracluster part

$$\begin{aligned} A_{c,k} &= \sqrt{p_c}\, a_{c,k}, \\ P_{c,k} &= p_c\, p_{c,k}, \\ \Phi_{c,k}^A &= \phi_c^A + \phi_{c,k}^A, \\ \Phi_{c,k}^D &= \phi_c^D + \phi_{c,k}^D, \\ T_{c,k} &= \tau_c + \tau_{c,k}. \end{aligned} \tag{3}$$

In (3), the parameters p_c, ϕ_c^A, ϕ_c^D, and τ_c denote *intercluster* propagation parameters and are representative for the *location* of each cluster in the power/AoA/AoD/delay parameter space. Also in (3), $a_{c,k}$, $p_{c,k}$, $\phi_{c,k}^A$, $\phi_{c,k}^D$, and $\tau_{c,k}$ are *intracluster* propagation parameters. The intracluster parameters can be seen as the deviations of individual paths from the cluster's location as dictated by the intercluster parameters. The intracluster parameters are therefore fully determined by the *spread* of power, AoA, AoD, and delay in

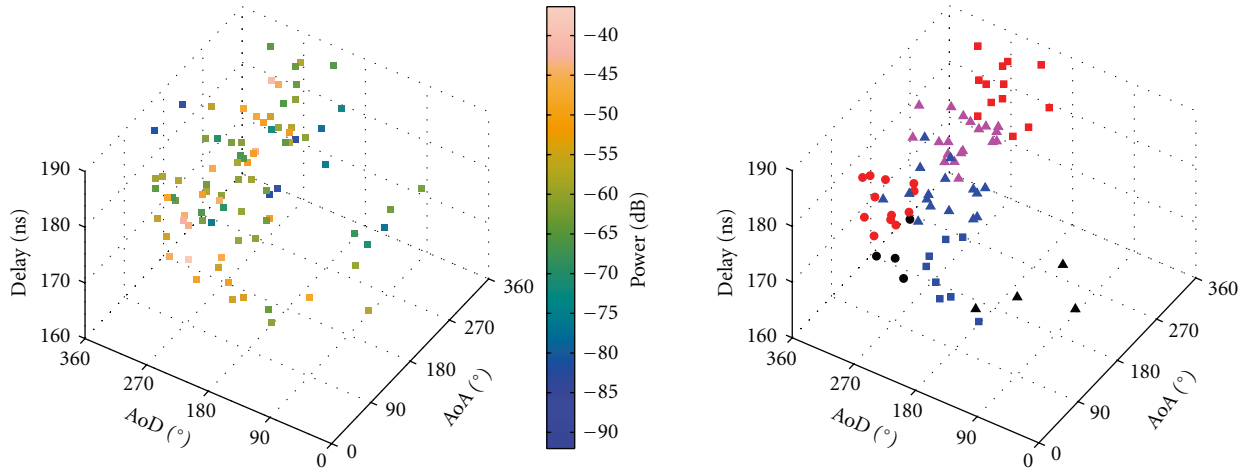

(a) MPC AoA/AoD/delay scatter plot

(b) MPC K-power-means clustering

Figure 4: MPC scatter plot and clustering for measurement location 1 (LoS).

each of the clusters. With the definitions in (3), the signal model in (1) is rewritten as

$$h\left(\phi^A,\phi^D,\tau\right)=\sum_{c=1}^{n_C}\sum_{k=1}^{n_{P,c}}\sqrt{p_c}a_{c,k}\cdot\delta\left(\phi^A-\phi_c^A-\phi_{c,k}^A\right)\times\delta\left(\phi^D-\phi_c^D-\phi_{c,k}^D\right)\delta(\tau-\tau_c-\tau_{c,k}). \tag{4}$$

Section 4 discusses the statistical distributions of $P_{c,k}$, $\Phi_{c,k}^A$, $\Phi_{c,k}^D$, and $T_{c,k}$ within each cluster. The most common probability distributions are location-scale distributions; they are parameterized by a location parameter, which determines the distribution's location or shift, and a scale parameter, which determines the distribution's dispersion or spread. These two types of distributional parameters can fully describe the intercluster and intracluster propagation parameters, and hence the signal model in (4); the distributional location parameter can be identified with the intercluster propagation parameter, and the distributional scale parameter fully characterizes the intracluster propagation parameter. The distributional location and scale parameters are further discussed in Section 5.

3.2. FABLE Notation. The goal of this section is to provide a new notation for the MIMO channel matrix. This notation is named *FActorization into a BLock-diagonal Expression* or *FABLE* [27, 28]. The appeal of the FABLE notation laid out here is in its future incorporation in the data model of multipath estimation algorithms. The FABLE notation further subdivides each of the angular and delay dimensions into an intra- and intercluster subdimension. This subdivision has the potential to further reduce the computational complexity of space-alternating estimation algorithms, as the harmonic retrieval problem is broken down into more dimensions. For appropriate antenna arrays at transmit and receive side, the transformation of (4) to aperture space is given by

$$\mathcal{H}(r,s,f)=\sum_{c=1}^{n_C}\sum_{k=1}^{n_{P,c}}\sqrt{p_c}a_{c,k}\cdot e^{-j2\pi(r-1)\mathrm{G}_{\mathrm{Rx}}(\phi_c^A+\phi_{c,k}^A)}\times e^{-j2\pi(s-1)\mathrm{G}_{\mathrm{Tx}}(\phi_c^D+\phi_{c,k}^D)}e^{-j2\pi f(\tau_c+\tau_{c,k})}. \tag{5}$$

In (5), the variables r, s, and f denote the transform variables of the Fourier transform of ϕ^A, ϕ^D, and τ, respectively. Each (integer) value of r and s can be associated with one of the antennas of the Rx and Tx antenna array. The variable f denotes the frequency of the transmitted signal. The functions $\mathrm{G}_{\mathrm{Rx}}(\cdot)$ and $\mathrm{G}_{\mathrm{Tx}}(\cdot)$ depend on the Rx and Tx array geometry. For example, $\mathrm{G}_{\mathrm{Rx}}(\cdot)=\mathrm{G}_{\mathrm{Tx}}(\cdot)=(d/\lambda)\sin(\cdot)$ for uniform linear arrays (ULAs) at receive and transmit side, where d is the spacing between antenna array elements, and λ is the wavelength.

In the following, it is assumed that the array geometry functions $\mathrm{G}_{\mathrm{Rx}}(\cdot)$ and $\mathrm{G}_{\mathrm{Tx}}(\cdot)$ are linear, that is, that in (5) it holds that $\mathrm{G}_{\mathrm{Rx}}(\phi_c^A+\phi_{c,k}^A)=\mathrm{G}_{\mathrm{Rx}}(\phi_c^A)+\mathrm{G}_{\mathrm{Rx}}(\phi_{c,k}^A)$ and analogously $\mathrm{G}_{\mathrm{Tx}}(\phi_c^D+\phi_{c,k}^D)=\mathrm{G}_{\mathrm{Tx}}(\phi_c^D)+\mathrm{G}_{\mathrm{Tx}}(\phi_{c,k}^D)$. Unfortunately, this assumption is usually not valid, for example, for the ULA, URA, and uniform circular array (UCA) geometries. This can be remedied by transforming the intercluster and intracluster angular propagation parameters. For example, for the receive side, the FABLE notation in the following can be used with ψ_c^A and $\psi_{c,k}^A$ as intercluster and intracluster AoA, respectively, for which it is satisfied that $\mathrm{G}_{\mathrm{Rx}}(\Phi_{c,k}^A)=\mathrm{G}_{\mathrm{Rx}}(\psi_c^A)+\mathrm{G}_{\mathrm{Rx}}(\psi_{c,k}^A)$. For example, for a ULA, this can be shown to hold if ψ_c^A and $\psi_{c,k}^A$ are defined such that $\sin(\psi_c^A)=\sin(\phi_c^A)\cos(\phi_{c,k}^A)$ and $\sin(\psi_{c,k}^A)=\cos(\phi_c^A)\sin(\phi_{c,k}^A)$. This transformation can be done without consequence as there an inherent arbitrariness on how the AoA is split up into its respective inter- and intracluster parts. The disadvantage of redefining the inter- and intracluster AoA is that $\Phi_{c,k}^A\neq\psi_c^A+\psi_{c,k}^A$, contrary to the definition with ϕ-s in (3).

This means that, unlike the definition with ϕ-s, the inter- and intracluster AoAs defined as ψ-s cannot be quickly related to the corresponding MPC AoA $\Phi_{c,k}^{A}$ and also depend on the array geometry function $\mathrm{G_{Rx}}(\cdot)$ under consideration.

We assume that the Rx and Tx antenna arrays consist of R and S antenna elements, respectively ($r = 1, \ldots, R$ and $s = 1, \ldots, S$). The MIMO channel transfer function $\mathcal{H}(r, s, f)$ is first rewritten as the MIMO channel matrix $\mathbf{H}(f)$. The channel matrix $\mathbf{H}$ has the common structure where the row dimension of $\mathbf{H}$ is made up from receive elements r and its column dimension is made up from transmit elements s ($\mathbf{H}$ has dimensions $R \times S$). The channel matrix $\mathbf{H}(f)$ is decomposed as the product of three matrices

$$\mathbf{H}(f) = \mathbf{B}^{\mathrm{Rx}}(f) \cdot \mathbf{W}(f) \cdot \mathbf{B}^{\mathrm{Tx}}. \tag{6}$$

In (6), $\mathbf{B}^{\mathrm{Rx}}(f)$ and $\mathbf{B}^{\mathrm{Tx}}$ contain intercluster propagation parameters associated with the Rx and Tx, respectively. By choice, the intercluster parameters p_c, ϕ_c^A, and τ_c are considered to be properties of cluster c as seen by the Rx, while ϕ_c^D is considered to characterize cluster c as seen from the Tx. Because of the choice to house delay τ_c in $\mathbf{B}^{\mathrm{Rx}}(f)$, the elements of this matrix depend on the frequency f. Also in (6), $\mathbf{W}(f)$ gathers the intracluster propagation parameters $a_{c,k}$, $\phi_{c,k}^A$, $\phi_{c,k}^D$, and $\tau_{c,k}$. The matrices $\mathbf{B}^{\mathrm{Rx}}$, $\mathbf{W}$, and $\mathbf{B}^{\mathrm{Tx}}$ are built from submatrices $\mathbf{B}_c^{\mathrm{Rx}}$, $\mathbf{W}_c$, and $\mathbf{B}_c^{\mathrm{Tx}}$, respectively, which contain the intercluster and intracluster propagation parameters solely associated with cluster c. The stacking of these submatrices is conceived as follows (the f dependency is left out for better readability):

$$\begin{aligned}\mathbf{H} &= \mathbf{B}^{\mathrm{Rx}} \cdot \mathbf{W} \cdot \mathbf{B}^{\mathrm{Tx}} \\ &= \begin{bmatrix} \mathbf{B}_1^{\mathrm{Rx}} & \mathbf{B}_2^{\mathrm{Rx}} & \cdots & \mathbf{B}_{n_C}^{\mathrm{Rx}} \end{bmatrix} \cdot \begin{bmatrix} \mathbf{W}_1 & \mathbf{0} & \cdots & \mathbf{0} \\ \mathbf{0} & \mathbf{W}_2 & \cdots & \mathbf{0} \\ \vdots & \vdots & \ddots & \vdots \\ \mathbf{0} & \mathbf{0} & \cdots & \mathbf{W}_{n_C} \end{bmatrix} \cdot \begin{bmatrix} \mathbf{B}_1^{\mathrm{Tx}} \\ \mathbf{B}_2^{\mathrm{Tx}} \\ \vdots \\ \mathbf{B}_{n_C}^{\mathrm{Tx}} \end{bmatrix}.\end{aligned} \tag{7}$$

The stacking of the submatrices $\mathbf{W}_c$ gives rise to a block-diagonal form for the intracluster matrix $\mathbf{W}$, from which the name FABLE is derived.

3.2.1. Intercluster Submatrices $\mathbf{B}_c^{\mathrm{Rx}}$ and $\mathbf{B}_c^{\mathrm{Tx}}$. For cluster c, the submatrices $\mathbf{B}_c^{\mathrm{Rx}}$ and $\mathbf{B}_c^{\mathrm{Tx}}$ have the following structure ($\mathrm{diag}(\cdot)$ represents a diagonal matrix with its arguments along the main diagonal):

$$\begin{aligned}\mathbf{B}_c^{\mathrm{Rx}} &= \sqrt{p_c} e^{-j2\pi f \tau_c} \\ &\quad \cdot \mathrm{diag}\left(1, e^{-j2\pi \mathrm{G_{Rx}}(\phi_c^A)}, \ldots, e^{-j2\pi(R-1)\mathrm{G_{Rx}}(\phi_c^A)}\right), \\ \mathbf{B}_c^{\mathrm{Tx}} &= \mathrm{diag}\left(1, e^{-j2\pi \mathrm{G_{Tx}}(\phi_c^D)}, \ldots, e^{-j2\pi(S-1)\mathrm{G_{Tx}}(\phi_c^D)}\right).\end{aligned} \tag{8}$$

It is clear that $\mathbf{B}_c^{\mathrm{Rx}}$ only contains intercluster propagation parameters associated with the Rx: the cluster mean AoA ϕ_c^A, the cluster onset τ_c at receive side, and the cluster median received power p_c. The submatrix $\mathbf{B}_c^{\mathrm{Tx}}$ contains the intercluster parameter associated with the Tx, that is, the cluster mean AoD ϕ_c^D. The submatrices $\mathbf{B}_c^{\mathrm{Rx}}$ and $\mathbf{B}_c^{\mathrm{Tx}}$ have dimensions $R \times R$ and $S \times S$, respectively.

3.2.2. Intracluster Submatrix $\mathbf{W}_c$. For cluster c, the submatrix $\mathbf{W}_c$ is written as the product of three matrices

$$\mathbf{W}_c = \mathbf{V}_c^{\mathrm{Rx}} \cdot \mathbf{D}_c^{\mathrm{Rx}} \cdot \mathbf{V}_c^{\mathrm{Tx}}. \tag{9}$$

The three matrices $\mathbf{V}_c^{\mathrm{Rx}}$, $\mathbf{D}_c^{\mathrm{Rx}}$ and $\mathbf{V}_c^{\mathrm{Tx}}$ possess the following structure

$$\begin{aligned}\mathbf{V}_c^{\mathrm{Rx}} &= \begin{bmatrix} 1 & 1 & \cdots & 1 \\ e^{-j2\pi \mathrm{G_{Rx}}(\phi_{c,1}^A)} & e^{-j2\pi \mathrm{G_{Rx}}(\phi_{c,2}^A)} & \cdots & e^{-j2\pi \mathrm{G_{Rx}}(\phi_{c,n_{P,c}}^A)} \\ \vdots & \vdots & \ddots & \vdots \\ e^{-j2\pi(R-1)\mathrm{G_{Rx}}(\phi_{c,1}^A)} & e^{-j2\pi(R-1)\mathrm{G_{Rx}}(\phi_{c,2}^A)} & \cdots & e^{-j2\pi(R-1)\mathrm{G_{Rx}}(\phi_{c,n_{P,c}}^A)} \end{bmatrix}, \\ \mathbf{D}_c^{\mathrm{Rx}} &= \mathrm{diag}\left(a_{c,1} e^{-j2\pi f(\tau_{c,1})}, a_{c,2} e^{-j2\pi f(\tau_{c,2})}, \ldots, a_{c,n_{P,c}} e^{-j2\pi f(\tau_{c,n_{P,c}})}\right), \\ \mathbf{V}_c^{\mathrm{Tx}} &= \begin{bmatrix} 1 & e^{-j2\pi \mathrm{G_{Tx}}(\phi_{c,1}^D)} & \cdots & e^{-j2\pi(S-1)\mathrm{G_{Tx}}(\phi_{c,1}^D)} \\ 1 & e^{-j2\pi \mathrm{G_{Tx}}(\phi_{c,2}^D)} & \cdots & e^{-j2\pi(S-1)\mathrm{G_{Tx}}(\phi_{c,2}^D)} \\ \vdots & \vdots & \ddots & \vdots \\ 1 & e^{-j2\pi \mathrm{G_{Tx}}(\phi_{c,n_{P,c}}^D)} & \cdots & e^{-j2\pi(S-1)\mathrm{G_{Tx}}(\phi_{c,n_{P,c}}^D)} \end{bmatrix}.\end{aligned} \tag{10}$$

$\mathbf{V}_c^{\mathrm{Rx}}$ and $\mathbf{V}_c^{\mathrm{Tx}}$ are Vandermonde matrices which contain for cluster c the intracluster AoAs $\phi_{c,k}^A$ and the intracluster AoDs $\phi_{c,k}^D$, respectively, ($k = 1, \ldots, n_{P,c}$). The diagonal matrix $\mathbf{D}_c^{\mathrm{Rx}}$ comprises the received intracluster complex amplitude $a_{c,k}$ and the intracluster delay $\tau_{c,k}$ ($k = 1, \ldots, n_{P,c}$). The matrices $\mathbf{V}_c^{\mathrm{Rx}}$, $\mathbf{D}_c^{\mathrm{Rx}}$, and $\mathbf{V}_c^{\mathrm{Tx}}$ have dimensions $R \times n_{P,c}$, $n_{P,c} \times n_{P,c}$, and $n_{P,c} \times S$, respectively.

As a closing remark, the FABLE notation in (7) can intuitively be understood as follows. Firstly, clusters with their average directional characteristics are created at transmit side by the matrix $\mathbf{B}^{\mathrm{Tx}}$. Next, the block-diagonal $\mathbf{W}$ matrix introduces several discrete paths into each cluster. The matrix $\mathbf{W}$ can be thought of as the operator which unfolds each cluster into its discrete paths. Finally, the matrix $\mathbf{B}_c^{\mathrm{Rx}}$ describes how the clusters' average directional characteristics are seen by the Rx when they arrive at receive side.

4. Statistics of the MPC Parameters

This section discusses the statistical distributions within each cluster of the MPC parameters $\Phi_{c,k}^A$, $\Phi_{c,k}^D$, $T_{c,k}$, and $P_{c,k}$. Preliminarily, the correlations between these four parameters are investigated to check whether they can be modelled separately by univariate distributions. A summary of this section's results is found in Table 2, near the end of the paper.

4.1. Correlations. In this section, correlations between azimuthal angles $\Phi_{c,k}^A$ and $\Phi_{c,k}^D$, delay $T_{c,k}$, and power $P_{c,k}$ are calculated. The measure of correlation used is Spearman's

Table 1: Average Spearman's correlation of MPC parameters within each cluster and success rates for zero correlation.

	Average Spearman's correlation [−]			Success rates at 5%/1% significance [%]		
	$\Phi^D_{c,k}$	$T_{c,k}$	$P_{c,k}$	$\Phi^D_{c,k}$	$T_{c,k}$	$P_{c,k}$
$\Phi^A_{c,k}$	0.04	−0.12	0.18	100.0/100.0	88.9/95.6	86.7/95.6
$\Phi^D_{c,k}$		−0.01	−0.09		95.6/100.0	95.6/100.0
$T_{c,k}$			−0.28			80.0/93.3

rank correlation coefficient [29]. This correlation coefficient is nonparametric in the sense that it does not make any assumptions on the form of the relationship between the two variables, other than being a monotonic relationship. Spearman's correlation is calculated between the four MPC parameters on a per-cluster basis. For the MPCs in cluster c, Spearman's correlation coefficient $\rho_c(X_{c,k}, Y_{c,k})$ between MPC parameters $X_{c,k}$ and $Y_{c,k}$ is given by ($X_{c,k}$, $Y_{c,k} = \Phi^A_{c,k}$, $\Phi^D_{c,k}$, $T_{c,k}$, or $P_{c,k}$)

$$\rho_c(X_{c,k}, Y_{c,k}) = 1 - \frac{6\sum_{k=1}^{n_{P,c}} \left(x_{c,k} - y_{c,k}\right)^2}{n_{P,c}\left(\left(n_{P,c}\right)^2 - 1\right)}. \tag{11}$$

In (11), $x_{c,k}$ and $y_{c,k}$ represent the statistical ranks of $X_{c,k}$ and $Y_{c,k}$. Before calculating their ranks, the azimuthal angle variables are restricted to their principal value in $(-\pi, \pi]$ to avoid the 2π ambiguity.

Table 1 shows average values of $\rho_c(X_{c,k}, Y_{c,k})$ taken over all 45 clusters detected in the measurement campaign. Table 1 shows fairly weak average correlations between the MPC parameters. The strongest correlation is found between path power $P_{c,k}$ and path delay $T_{c,k}$ (negative average correlation of −0.28). This correlation is expected and well established by the Saleh-Valenzuela model, where power decay within a cluster is modeled as a monotonically decreasing exponential function of delay [30]. For all $\rho_c(X_{c,k}, Y_{c,k})$, hypothesis tests (nonparametric permutation tests) are carried out to decide whether or not the correlation coefficients differ significantly from zero. Table 1 lists the success rates of these tests, that is, for which percentage of clusters the test decided in favor of zero correlation, at both the 5% and 1% significance level. Table 1 shows that, for most clusters, the MPC parameter correlations can be assumed to be zero (success rates of more than 80% and more than 93% at the 5% and 1% significance level, resp.). As expected, the success rates are the lowest for correlation between $P_{c,k}$ and $T_{c,k}$, for which the strongest correlation was found. Concluding, correlations between MPC parameters within clusters can be assumed to be weak and often indistinguishable from zero. Therefore, the MPC parameters $\Phi^A_{c,k}$, $\Phi^D_{c,k}$, $T_{c,k}$, and $P_{c,k}$ are modelled separately by univariate distributions in the next sections, without taking any relationships between them into account.

Alternatively, correlation coefficients can also be calculated with the parametric circular-linear and circular-circular correlation coefficients defined in [31]. These correlation coefficients are designed to work with circular data (in our case, the azimuthal angles). Using these correlation coefficients, average correlation values are somewhat larger than those for Spearman's correlation in Table 1 and range from −0.27 to 0.49. Hypothesis tests for zero correlation at the 5% significance level however still deliver success rates of more than 84%, supporting the previous decision of modelling the MPC parameters univariately.

4.2. Azimuths of Arrival $\Phi^A_{c,k}$ and Departure $\Phi^D_{c,k}$. In this section, we discuss the marginal distributions of AoAs $\Phi^A_{c,k}$ and AoDs $\Phi^D_{c,k}$ for each individual cluster c. In literature, various distributions are proposed for the azimuth angles within a certain cluster. In [9], a normal distribution is chosen where realisations are mapped to their principal value in $(-\pi, \pi]$. A Laplacian distribution for the azimuth angles is first proposed in [32]. Additionally, we consider the von Mises distribution [33]. The von Mises distribution can be thought of as an analogue of the normal distribution for circular data. Special consideration is given to this distribution, because in our opinion, the von Mises distribution seems natural in describing the statistics of azimuth data; the support of the von Mises distribution is an interval of length 2π, the same as the support of azimuth data, while the support of the normal and Laplacian distribution is an interval of infinite length. For example, for the AoAs $\Phi^A_{c,k}$ in cluster c, the von Mises probability density function (pdf) $\mathrm{p_{vM}}(\Phi^A_{c,k}\ ;\ \alpha^A_c, \kappa^A_c)$ is given as

$$\mathrm{p_{vM}}\left(\Phi^A_{c,k}\ ;\ \alpha^A_c, \kappa^A_c\right) = \frac{\exp\left(\kappa^A_c \cos\left(\Phi^A_{c,k} - \alpha^A_c\right)\right)}{2\pi \mathrm{I}_0\left(\kappa^A_c\right)}, \quad k = 1, \ldots, n_{P,c}. \tag{12}$$

In (12), $\mathrm{I}_0(\cdot)$ is the modified Bessel function of the zeroth order. The two parameters that characterize the von Mises pdf are α^A_c, the circular mean of $\Phi^A_{c,k}$, and κ^A_c, which is a measure of concentration of $\Phi^A_{c,k}$ angles around α^A_c.

The most fit distributions for the intracluster AoAs and AoDs are investigated as follows. From the azimuth angles $\Phi^A_{c,k}$ and $\Phi^D_{c,k}$, the maximum likelihood estimators (MLEs) of the parameters of the normal, Laplacian, and von Mises pdf are calculated separately for the AoAs and AoDs of each cluster c. For cluster c, the likelihood of observing the samples $\Phi^A_{c,k}$ (analogously $\Phi^D_{c,k}$) for $k = 1, \ldots, n_{P,c}$ as possible outcomes under each of the three statistical distributions (with the MLEs as distributional parameters) is calculated. The most fit distribution is determined by performing simple likelihood ratio tests (LRTs); the statistical distribution which renders the largest likelihood is most appropriate for describing the azimuth angle statistics for that cluster. For the 45 clusters in this measurement campaign, all LRTs decided in favor of the von Mises distribution for both $\Phi^A_{c,k}$ and $\Phi^D_{c,k}$. Figure 5 shows the empirical cumulative distribution function (CDF) of the AoAs $\Phi^A_{c,k}$ of a cluster at measurement location 5. Also shown are the estimated CDFs of the Von Mises, normal, and Laplacian distribution. Visually, it could be concluded from Figure 5 that all three investigated theoretical distributions provide a reasonable fit to the empirical data, and that any of these distributions

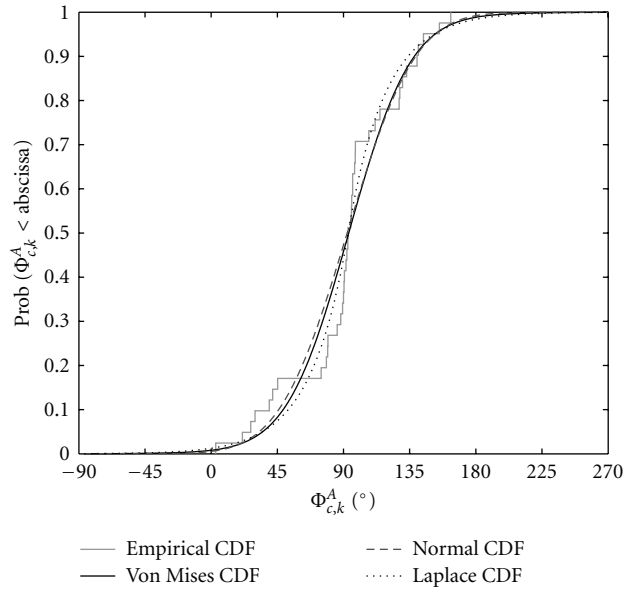

FIGURE 5: CDF plot of $\Phi^A_{c,k}$ and estimated theoretical CDFs for a cluster at measurement location 5.

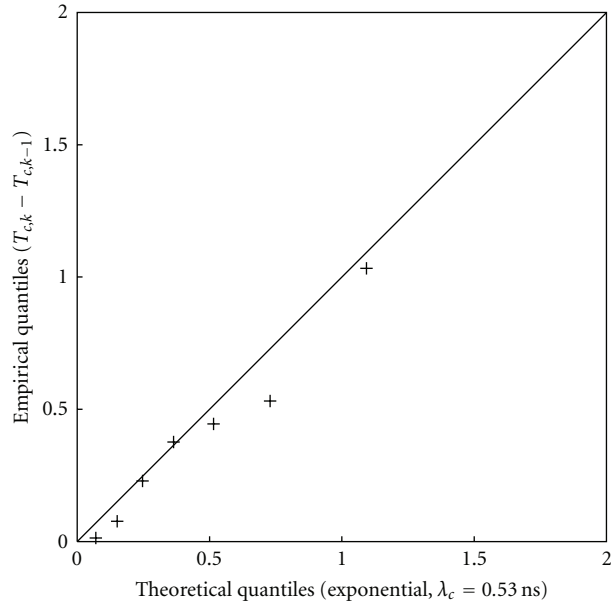

FIGURE 6: QQ plot of quantiles of $T_{c,k} - T_{c,k-1}$ versus quantiles of an exponential distribution for a cluster at measurement location 3.

could be chosen for modelling the AoA. However, the LRTs allow to quantitatively measure the goodness of fit and decide in favor of the von Mises distribution.

4.3. Delay $T_{c,k}$. In this section, the statistics within each cluster c of the delay parameter $T_{c,k}$ are discussed. The marginal distribution of the delay parameter can be modeled in a number of ways. In [9], MPC delays within a cluster are assumed to be normally distributed. A possible issue with this modeling approach is that MPC delays inherently only take on positive values, which does not match the support of the normal distribution. To avoid this issue, MPC delays $T_{c,k}$ within cluster c are modelled according the principle laid out by the well-known, cluster-based Saleh-Valuenzuela (SV) model [30]. Herein, the waiting time between the arrival of two consecutive MPCs within a certain cluster is modelled by an exponential distribution. For the MPCs in cluster c (assuming the delays are ordered such that $T_{c,1} < T_{c,2} < \cdots < T_{c,n_{P,c}}$), the exponential pdf $\mathrm{p}_{\exp}(T_{c,k} \mid T_{c,k-1}; \lambda_c)$ as function of the delay $T_{c,k}$ of the kth MPC, given that the $(k-1)$th MPC arrived at known delay $T_{c,k-1}$, is written as

$$\mathrm{p}_{\exp}(T_{c,k} \mid T_{c,k-1}\ ;\ \lambda_c) = \frac{1}{\lambda_c} \exp\left(-\frac{T_{c,k} - T_{c,k-1}}{\lambda_c}\right), \quad k = 2, \ldots, n_{P,c}. \tag{13}$$

In (13), the exponential distribution has the parameter λ_c which corresponds to the mean waiting time between consecutive MPCs in cluster c. An additional distributional parameter θ_c is defined as the delay of the first arriving path in cluster c, that is, $\theta_c = T_{c,1}$, as $T_{c,1}$ does not follow from (13).

For each cluster c, the mean waiting time λ_c is estimated by its MLE following from the exponential distribution. The plausibility of an exponential distribution for the arrival times $T_{c,k}$ is then validated by executing an Anderson-Darling (AD) goodness-of-fit test for composite exponentiality [34]. For the 45 clusters in the measurement campaign, the minimum, average, and maximum P values associated with the AD test are equal to .06, .40, and .92, respectively. This means that, at the 5% significance level, all 45 clusters retain exponentiality. Figure 6 shows the quantile-quantile (QQ) plot of the empirical quantiles of samples $T_{c,k} - T_{c,k-1}$ versus the theoretical quantiles of the exponential distribution (13) for a cluster detected at measurement location 3 (the MLE of λ_c equals 0.53 ns). Figure 6 shows good agreement of the waiting times in this cluster with an exponential distribution.

4.4. Power $P_{c,k}$. A natural model for the fading of MPC powers $P_{c,k}$ in cluster c is the lognormal fading model [35, 36]. For cluster c, it is investigated whether the samples $P_{c,k}$ on a dB scale could originate from a normal distribution. This normal distribution is parameterized by the mean μ_c and the standard deviation σ_c of $P_{c,k}$ in dB. These distributional parameters are estimated by their MLEs.

Composite normality of $P_{c,k}$ [dB] is assessed with a few statistical tests in literature such as the Anderson-Darling (AD) test [34], the Shapiro-Wilk (SW) test [37], and the Henze-Zirkler (HZ) test [38]. Multiple tests for normality are executed as no uniformly most powerful test exists against all possible alternative distributions. The AD, SW, and HZ tests are generally considered to be relatively powerful against a variety of alternatives. Of the 45 clusters in this measurement campaign, normality of $P_{c,k}$ [dB] is retained at the 5% significance level for 39, 38, and 40 clusters with the AD, SW, and HZ tests, respectively. For the 45 clusters, average P values are .38 (AD), .43 (SW), and .44 (HZ). Concluding,

normality for $P_{c,k}$ [dB] is assumed in the following, as the majority of clusters pass the different goodness-of-fit tests.

5. Statistics of the Distributional Parameters

This section models the intercluster and intracluster propagation parameters laid out in the signal model of Section 3 in (1), (3), and (4). The intercluster and intracluster propagation parameters are fully determined by the distributional parameters of the location-scale distributions of the previous section. In the following, the intercluster propagation parameters are identified with the location parameters of the distributions, that is, for cluster c,

$$\begin{aligned}
\phi_c^A &\triangleq \alpha_c^A \ \text{(von Mises circular mean of AoAs)},\\
\phi_c^D &\triangleq \alpha_c^D \ \text{(von Mises circular mean of AoDs)},\\
\tau_c &\triangleq \theta_c \ \text{(onset of delays)},\\
p_c &\triangleq \mu_c \ \text{(normal mean of powers in dB)}.
\end{aligned} \tag{14}$$

The intracluster propagation parameters are characterized by the scale parameters of the distributions, that is, for the MPCs in cluster c,

$$\begin{aligned}
\phi_{c,k}^A &\longrightarrow \kappa_c^A \ \text{(von Mises concentration of AoAs)},\\
\phi_{c,k}^D &\longrightarrow \kappa_c^D \ \text{(von Mises concentration of AoDs)},\\
\tau_{c,k} &\longrightarrow \lambda_c \ \text{(exponential mean waiting time between delays)},\\
p_{c,k} &\longrightarrow \sigma_c \ \text{(normal standard deviation of powers in dB)}.
\end{aligned} \tag{15}$$

In the following, the statistics of the distributional parameters are discussed. Preliminarily, correlations between these parameters are investigated. In this section, distinction is made between distributional parameters originating from LoS and nLoS measurements, and it is assessed whether the parameters' statistics differ significantly between LoS and nLoS. A summary of this section's results is found in Table 2.

5.1. Correlations. Spearman's rank correlation coefficient is calculated between the location and scale parameters, and the two number parameters n_C and $n_{P,c}$. 45 samples for each of these parameters are available (45 clusters in this campaign). Figures 7(a) and 7(b) show the upper triangles of the correlation matrices of estimated parameters stemming from LoS and from nLoS measurements. Permutation tests are carried out to decide on the significance of each of the correlations. Correlation coefficients which prove to significantly differ from zero at a 5% level are marked with the text "5%." Correlation coefficients which are different from zero at the more strict 1% significance level are marked with a "1%" label. For correlations without a label, the permutation test accepted the hypothesis of zero correlation at the 5% significance level.

Firstly, we look at the correlations between the distributional parameters in (14) and (15) (part of the correlation matrices inside the dashed rectangles in Figures 7(a) and 7(b)). Most notably, the correlation between cluster mean power p_c and cluster onset τ_c proves to be strong at the 1% significance level, and this for both LoS (negative correlation of -0.80, P value of $1.8 \cdot 10^{-4}$) and nLoS (negative correlation of -0.58, P value of $9.7 \cdot 10^{-4}$). This is well established in the Saleh-Valenzuela model, where linear cluster power is modelled as exponentially decaying with cluster delay [30]. This strong correlation cannot be easily ignored, so p_c is modelled through regression with τ_c in the following. Additionally, in Figure 7, some correlations are significant at the 5% level but not at the 1% level. These correlations can sometimes be explained from the expected propagation physics; for example, regarding the positive correlation of 0.37 between σ_c and λ_c in nLoS, it is expected that the variability of MPC power σ_c will be larger if the MPCs are characterized by a larger λ_c, that is, have delays that are further in between. For simplicity of the provided models, we choose to not perform regression between distributional parameters for which the correlation is significant at the 5% level but not at the 1% level, also because these correlations are between different distributional parameters for LoS and nLoS. Summarizing, the distributional parameters will be modelled by their marginal statistical distributions in the next sections, except for the mean cluster power p_c which strongly depends on the cluster onset τ_c.

Secondly, we look at the correlations with the number parameters n_C and $n_{P,c}$ (part of the correlation matrices outside the dashed rectangles in Figures 7(a) and 7(b)). In this paper, no model is provided for the number of paths per cluster $n_{P,c}$; MPC parameter extraction in Section 2.3.1 estimated the 100 strongest MPCs without deciding on the actual number of paths through heuristics. Nevertheless, the significant correlations with $n_{P,c}$ in Figure 7 can give information about the effect of the number of paths per cluster on the estimation accuracy of other cluster parameters, in particular scale (dispersion) parameters. For example, at the 1% level, the correlation between $n_{P,c}$ and λ_c is significant for both LoS (negative correlation of -0.73) and nLoS (negative correlation of -0.61). As clusters contain paths with similar delay characteristics, it can be expected that a larger number of paths $n_{P,c}$ will yield closer spacing of these paths on the delay axis, that is, smaller estimated values of λ_c. In contrast to this, the estimation of the other scale parameters κ_c^A, κ_c^D, and σ_c does not seem to be greatly affected by $n_{P,c}$. In Figure 7(a), the number of clusters n_C is not strongly correlated with the distributional parameters for the LoS measurements. In Figure 7(a), for nLoS, the correlation between n_C and the location ϕ_c^A of the clusters on the AoA axis is significant at the 5% level (negative correlation of -0.39). However, as there is no physical basis to assume that the arrival angle of a cluster should depend on the total number of arriving clusters, this correlation will not be taken into account while modelling the statistics of n_C.

From the data in Figure 7, the conclusion is that a majority of the correlations can be assumed to be zero, which means that the multivariate postulation can be weakened

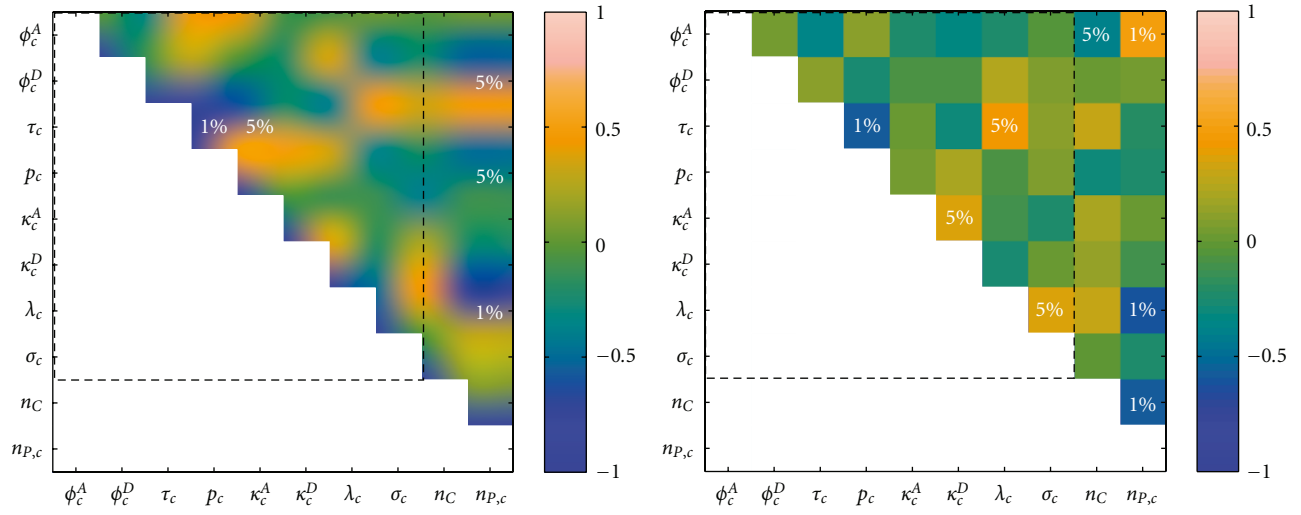

(a) LoS measurements

(b) nLoS measurements

Figure 7: Spearman's correlation of distributional and number parameters

without completely moving to the univariate assumption. Future work on this topic is to investigate whether or not omitting correlations which are assumed to be zero would significantly degrade channel matrix estimates. Finally, we compare the correlation analysis in this section with the observations made in [39]. In this work, strong correlations between spreads in the AoA, AoD, and delay domains are found, that is, clusters are small or large in all domains at once. These strong correlations are not found for our measurements (see the correlations between the scale parameters in Figure 7), except for LoS where κ_c^A and κ_c^D show significant correlation. Contrary to [39], where an LoS/obstructed LoS scenario is considered, our measurements also include a heavy nLoS scenario with propagation through walls. For our nLoS case, cluster spreads in all domains appear to be decorrelated. For our LoS case, the azimuthal spreads are significantly correlated as in [39]. However, in contrast to this work, correlation with delay spread is weak for our measurements, which is likely caused by our LoS cases being restricted to hallway propagation.

5.2. Location Parameters (Intercluster)

5.2.1. Cluster Angular Means ϕ_c^A and ϕ_c^D. The uniform distribution is a suitable distribution for modelling ϕ_c^A and ϕ_c^D, as from a modelling perspective there is no physical basis for a certain mean AoA or AoD to have a higher probability of occurrence than another mean AoA or AoD. In this section, no distinction is made between LoS and nLoS, because the uniform distribution is not parameterized by any distributional parameter (which could change between these two circumstances). The premise of a uniform distribution in $(-\pi, \pi]$ for the intercluster mean azimuth angles is validated through statistical hypothesis tests. In [7], the popular Kolmogorov-Smirnov (KS) test is advocated for goodness of fit of the propagation parameters' underlying distributions. However, for small sample sizes, the KS test is known to have low power. Because of this, we use Rao's spacing test for uniformity [40]. This test has the following advantages over the KS test: it is designed for circular data, has higher power, and is nonparametric which means that no error-prone distributional assumption is made on the test statistic. For both the 45 cluster mean AoAs ϕ_c^A and the 45 cluster mean AoDs ϕ_c^D, Rao's spacing test retained the null hypothesis of a uniform distribution in $(-\pi, \pi]$ at the 5% significance level (P values of .67 and .14, resp.).

5.2.2. Cluster Onset τ_c. For consistency with the modelling of the intracluster delay in Section 4.3, we also adopt the Saleh-Valenzuela model for the intercluster delay; the waiting time between the onsets $\tau_c - \tau_{c-1}$ of two consecutively arriving clusters is modelled by an exponential distribution [30]. This exponential distribution is fully parameterized by the mean of waiting times $\tau_c - \tau_{c-1}$. Under the assumption of an exponential distribution, it is first investigated whether the mean waiting time between clusters differs between LoS and nLoS measurements. This is done by executing the two-sample Anderson-Darling (AD) test, which assesses whether $\tau_c - \tau_{c-1}$ grouped according to LoS or nLoS could both originate from the same statistical distribution. This test results in a P value of .04, which is borderline significant at the 5% level and prompts us to distinguish between LoS and nLoS. Next, for LoS and nLoS separately, composite exponentiality of $\tau_c - \tau_{c-1}$ is verified using the one-sample AD test. An exponential distribution is accepted for both LoS and nLoS at the 5% significance level (P values of .13 and .12, resp.). The mean of waiting times $\tau_c - \tau_{c-1}$ is estimated at 2.30 ns for LoS and 1.21 ns for nLoS (see Table 2). Clusters seem to arrive in more rapid succession in nLoS than in LoS, which could be due to the choice of measurement locations in Figure 2. For the nLoS measurements, at least either the Tx or Rx are located in an office, while the LoS measurements are strictly hallway to hallway propagation. The offices have smaller dimensions and contain more closely spaced groups

of scatterers (desks, etc.) than the hallway, which renders them more likely to produce clusters closer in the delay domain.

Other measurement campaigns in office environments which used the Saleh-Valenzuela model found mean waiting times between cluster onsets ranging from 27 to 60 ns [41, 42]. These larger values compared to our measurements could be attributed to the fact that measurements in literature clustered propagation paths based only on path delay. The two extra dimensions (two azimuth angles) used in our clustering procedure increases the discriminatory power of the clustering, that is, more clusters can be distinguished between. It is therefore expected that joint AoA/AoD/delay clustering results in clusters more closely spaced in the delay domain.

5.2.3. Cluster Mean Power p_c. For both LoS and nLoS, significant correlation was found between cluster mean power p_c and cluster onset τ_c in Section 5.1. In literature, two commonly used models exist for the monotonic decay of p_c with increasing τ_c. The first model (Saleh-Valenzuela model) proposes a linear decrease of the average p_c of MPC powers in dB with the cluster onset τ_c (exponential law) [30]. The second model proposes a linear decrease of p_c in dB with the logarithm of τ_c (power law) [35],

$$p_c\,[\mathrm{dB}] = a_0 + a_1 \cdot \tau_c\,[\mathrm{ns}] + a_2 \cdot D_c + a_3 \cdot \tau_c\,[\mathrm{ns}] \cdot D_c + \epsilon_c \ \text{(exponential law)}, \tag{16}$$

$$p_c\,[\mathrm{dB}] = b_0 + b_1 \cdot 10\log(\tau_c\,[\mathrm{ns}]) + b_2 \cdot D_c + b_3 \cdot 10\log(\tau_c\,[\mathrm{ns}]) \cdot D_c + \chi_c \ \text{(power law)}. \tag{17}$$

In the models (16) and (17), p_c (in dB) is made dependent on τ_c (in ns) or $10\log(\tau_c)$ (in dBns) and the dummy variable D_c. The value of D_c is one for clusters stemming from LoS measurements and is zero for nLoS clusters. The terms ϵ_c and χ_c denote the models' errors for cluster c and are generally assumed to be zero-mean normally distributed. The regression parameters a_0 through a_3 and b_0 through b_3 are estimated using a backward elimination procedure [43]:

$$\begin{aligned} a_0 &= -20.14\,\mathrm{dB}, \quad a_1 = -0.81\,\mathrm{dB/ns}, \\ a_2 &= 0\,\mathrm{dB}, \quad a_3 = 0\,\mathrm{dB/ns}\,(\text{exponential law}), \\ b_0 &= -22.35\,\mathrm{dB}, \quad b_1 = -0.55, \\ b_2 &= 0\,\mathrm{dB}, \quad b_3 = 0\ (\text{power law}). \end{aligned} \tag{18}$$

The standard deviations of ϵ_c in (16) and χ_c in (17) are estimated at 4.72 dB and 5.09 dB, respectively. In (18), it is noted that the regression parameters a_2, a_3, b_2, and b_3 associated with the dummy variable D_c are assumed to be zero at the 5% significance level by the backward elimination procedure. This means that the form of the exponential and power law models is not significantly different between LoS and nLoS measurements. The coefficients of determination for the exponential and power law models are equal to 0.42 and 0.26, respectively. The exponential law model is therefore preferred as it explains a larger part of the variability of p_c than the power law model. Figure 8 shows a scatter plot of p_c versus τ_c along with the fitted exponential law model (16). The exponential law model is also shown in Table 2.

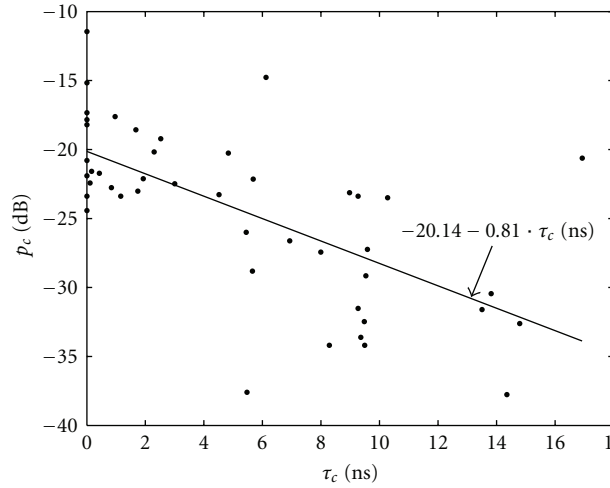

Figure 8: Scatter plot of p_c versus τ_c and fitted exponential law model.

5.3. Scale Parameters (Intracluster). This section discusses the statistics of the distributional scale parameters in (15). To our knowledge, no examples of possible statistical distributions for the scale parameters exist in literature. We will therefore use the entropy-maximizing normal distribution to model these parameters. As the scale parameters can only take on positive values, they are first log transformed to match the support of the normal distribution (i.e., any positive or nonpositive number). Also, log transformation has the additional benefit of softening the impact of outliers (large values of the scale parameters), which makes it more probable that log transformed variables are well described by a normal distribution. In the next sections, the premise of a normal distribution is investigated for the log-transformed scale parameters $\log(\kappa_c^A)$, $\log(\kappa_c^D)$, $\log(\lambda_c)$, and $\log(\sigma_c)$.

5.3.1. Cluster Angular Concentrations κ_c^A and κ_c^D. For both κ_c^A and κ_c^D, the two-sample Anderson-Darling (AD) test detects no difference between LoS and nLoS distributions at the 5% significance level (P values of .16 and .20, resp.). Without making distinction between LoS and nLoS, the assumptions of normality for $\log(\kappa_c^A)$ and $\log(\kappa_c^D)$ are validated using the statistical tests of Section 4.4: the Anderson-Darling (AD), Shapiro-Wilk (SW), and Henze-Zirkler (HZ) tests. For $\log(\kappa_c^A)$, all three tests accepted normality at the 5% level with P values of .37 (AD), .46 (SW), and .31 (HZ). The sample mean and sample standard deviation of $\log(\kappa_c^A)$ are equal to 0.50 and 0.33, respectively (see Table 2). Furthermore, normality is also accepted for $\log(\kappa_c^D)$ with P values of .09 (AD), .14 (SW), and .59 (HZ). The sample

mean and standard deviation of $\log(\kappa_c^D)$ equal 0.36 and 0.32, respectively (see Table 2).

The concentration parameters κ_c^A and κ_c^D range from 0.42 to 14.73 and from 0.46 to 16.25. For comparison, the von Mises distribution is also proposed for the non-isotropic angular dispersion in outdoor suburban/urban environments in [33]. Herein, the concentration of AoAs perceived by a mobile antenna below rooftop height ranges from 0.6 to 3.3. Compared to our measurement campaign, the AoAs seem to be somewhat less concentrated in outdoor environments, which could be explained from the larger physical structures in outdoor environments which cause scattering in a broader angular range.

5.3.2. Cluster Mean Waiting Time between MPCs λ_c. It is first assessed whether λ_c (in ns) originating from LoS or nLoS measurements could have been drawn from the same statistical distribution. A two-sample AD test on λ_c grouped according to LoS or nLoS results in a P value of .19, indicating no significant difference between LoS and nLoS at the 5% level. Next, normality for $\log(\lambda_c)$ without making distinction between LoS and nLoS is considered: AD, SW, and HZ hypothesis tests accepted normality at the 5% level with P values of .13, 0.21, and .13, respectively. We therefore assume a normal distribution for $\log(\lambda_c)$; the sample mean and sample standard deviation of $\log(\lambda_c)$ are equal to 0.03 and 0.35, respectively (see Table 2).

The parameter λ_c varies from 0.23 ns to 6.99 ns between the clusters of all executed MIMO measurements and is equal to 1.52 ns on average. For comparison, measurements in [41] yielded an average λ_c of about 0.16 ns (estimation of MPC delay using the frequency domain maximum likelihood or FDML procedure), while measurements in [42] resulted in an average λ_c of 4 ns (estimation of MPC delay using the inverse discrete Fourier transform or IDFT procedure). These results correspond well with our average λ_c of 1.52 ns, despite that MPC delay is estimated differently using the ESPRIT procedure.

5.3.3. Cluster Standard Deviation of Power σ_c. For σ_c (in dB), a two-sample AD test decides that there is no significant change in the statistical distribution of this parameter between LoS and nLoS measurements (P value of .34). Normality for $\log(\sigma_c)$ is assessed with the AD, SW, and HZ hypothesis tests, all of which accepted normality at the 5% level (P values of .61, .78, and .41, resp.). The sample mean and sample standard deviation of $\log(\sigma_c)$ are equal to 0.88 and 0.14, respectively (see Table 2). Figure 9 shows a QQ plot of empirical quantiles of $\log(\sigma_c)$ versus theoretical quantiles of a uniform distribution; good agreement between both can be seen.

5.4. Number of Clusters. In literature, the number of clusters n_C in geometry-based stochastic channel models, is characterized in various ways. In [9], the probability density function of n_C follows from marginalizing a continuous multivariate distribution. A possible issue with this approach is that samples of n_C drawn from a continuous distribution

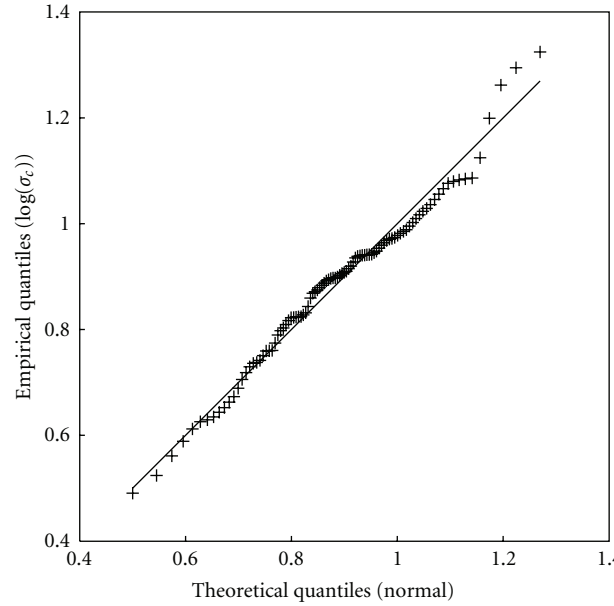

Figure 9: QQ plot of quantiles of $\log(\sigma_c)$ versus quantiles of a normal distribution.

have to be rounded to integer values, as n_C is a discrete variable. For other channel models the number of clusters is fixed. For example, in [6], n_C is equal to 6, while in [7], n_C in indoor office environments is assumed to be 12 in LoS conditions and 16 in nLoS conditions. In [19], the number of clusters is modeled by a discrete probability distribution, n_C is found to be a minimum value of 3 plus a Poisson-distributed random variable. Herein, the mean number of clusters is found equal to 4.69. The number of clusters varies to some extent between reports in literature, this is however expected, as the number of cluster will greatly depend on the adopted definition of clusters and the sort of clustering algorithm used.

For our measurements, there is no significant difference in the statistical distribution of n_C between LoS and nLoS, as concluded by a two-sample AD test at the 5% level (P value of .87). As in [19], the Poisson distribution is also adopted here for the number of clusters n_C, as it is a natural candidate distribution for the number of events occurring in a specified (time) interval. For example, the Poisson distribution has already been applied to the number of paths characterization problem in [44]. The minimum number of clusters for the K-power-means clustering algorithm in Section 2.3.2 is set to 2. Therefore, the number of clusters n_C is modelled as a minimum value of 2 plus a Poisson-distributed random variable. The probability density function $\mathrm{p}_{\mathrm{Poiss}}(n_C;\eta)$ of n_C is written as

$$\mathrm{p}_{\mathrm{Poiss}}(n_C;\eta) = \frac{(\eta-2)^{n_C-2}e^{-(\eta-2)}}{(n_C-2)!}, \quad n_C \geq 2. \tag{19}$$

In (19), the distributional parameter η is the mean number of detected clusters. The MLE for η is the sample mean of n_C and equals 5.00 for our measurements (see Table 2). This value is comparable to a mean number of

Table 2: Summary of statistical modelling of MPC parameters with clustering.

MPC parameter	Intracluster distribution	Intercluster (bc) and Intracluster (wc) parameters	Statistical modelling
AoA $\Phi_{c,k}^{A}$ [rad]	von Mises	(bc) ϕ_c^A [rad]	*Uniformly distributed*
		(wc) κ_c^A [−]	*Lognormally distributed* Mean of $\log(\kappa_c^A) = 0.50$ Standard deviation of $\log(\kappa_c^A) = 0.33$
AoD $\Phi_{c,k}^{D}$ [rad]	von Mises	(bc) ϕ_c^D [rad]	*Uniformly distributed*
		(wc) κ_c^D [−]	*Lognormally distributed* Mean of $\log(\kappa_c^D) = 0.36$ Standard deviation of $\log(\kappa_c^D) = 0.32$
delay $T_{c,k}$ [ns]	Exponential	(bc) τ_c [ns]	*Exponentially distributed* Mean of $\tau_c - \tau_{c-1} = 2.30$ ns (los)/1.21 ns (nlos)
		(wc) λ_c [ns]	*Lognormally distributed* Mean of $\log(\lambda_c) = 0.03$ Standard deviation of $\log(\lambda_c) = 0.35$
power $P_{c,k}$ [−]	Lognormal	(bc) p_c [dB]	$p_c[\text{dB}] = -20.14 - 0.81 \cdot \tau_c[\text{ns}] + \epsilon_c$ ϵ_c zero-mean normally distributed with standard deviation 4.72 dB
		(wc) σ_c [dB]	*Lognormally distributed* Mean of $\log(\sigma_c) = 0.88$ Standard deviation of $\log(\sigma_c) = 0.14$
	Number parameter	Statistical modelling	
	Number of clusters n_C [−]	*Poisson distributed* mean of $n_C = 5.00$	

clusters equal to 4.69 found in [19]. Herein, clustering is also done with the K-power-means algorithm and by using the Kim-Parks index. A Kolmogorov-Smirnov goodness-of-fit test accepted the Poisson distribution for n_C in (19) at the 5% significance level with a P value of .50.

6. Summary

In this paper, directional MIMO measurements in an indoor office environment are presented. Measurements are performed through frequency-domain channel sounding in the 3.5 GHz band. The spatial structure of the channel is captured by 10 by 4 uniform rectangular antenna arrays at both link ends. The antenna arrays are created using the virtual array technique. From these measurements, parameters associated with discrete propagation paths are extracted using a joint 5D ESPRIT estimation algorithm. The estimated path parameters include azimuth of arrival, azimuth of departure, delay, and power. In agreement with the geometry-based stochastic type of MIMO channel models, the path parameters are grouped into clusters using the statistical K-power-means algorithm.

Statistical distributions of the propagation parameters within individual clusters are determined, and correlations between these parameters are assessed. Motivated choices for the statistical distributions are made, based on the propagation physics expected in office environments. For example, the von Mises distribution for circular data is chosen for the statistics of the azimuth angles of arrival and departure. The distributional location and scale parameters are subsequently used to characterize the intracluster and intercluster dynamics of the propagation path parameters. This is done by in turn determining the statistical distributions of these location and scale parameters, and considering their correlations. To validate the distributional choices made in this paper, the goodness of fit to the proposed distributions is verified using a number of statistical hypothesis tests with sufficient power. The most important results of the statistical analysis are summarized in Table 2.

Additionally, a new notation for the MIMO channel matrix is given which more visibly shows the clustered nature of propagation paths. This notation is named *FActorization into a BLock-diagonal Expression* or *FABLE*. Future work includes the use of FABLE as the signal model in multipath estimation algorithms such as ESPRIT. The conventional signal model of these algorithms currently does not take clustering into account.

Acknowledgments

W. Joseph is a Postdoctoral Fellow of the FWO-V (Research Foundation—Flanders). This work was carried out within the frame of CISIT (International Campus on Safety and Intermodality in Transportation) and with the support of the FEDER funds, the French Ministry of research and the Region Nord Pas-de-Calais (France).

References

[1] "Wireless LAN Medium Access Control (MAC) and Physical Layer (PHY) specifications—Amendment 4: Enhancements for Higher Throughput," IEEE P802.11 Task Group, 2009, http://www.ieee802.org/11/.

[2] "Air Interface for Fixed and Mobile Broadband Wireless Access Systems—Amendment 2: Physical and Medium Access Control Layers for Combined Fixed and Mobile Operation in Licensed Bands," IEEE 802.16 Working Group on Broadband Wireless Access Standards, 2006, http://www.ieee802.org/16/.

[3] 3rd Generation Partnership Project, "Physical Layer Aspect for Evolved Universal Terrestrial Radio Access (UTRA)," Tech. Rep. 3GPP TR 25.814 v7.1.0, 2006, http://www.3gpp.org/.

[4] C. Oestges and B. Clerckx, *MIMO Wireless Communications: From Real-World Propagation to Space-Time Code Design*, Academic Press, 1st edition, 2007.

[5] J. J. Blanz and P. Jung, "A flexibly configurable spatial model for mobile radio channels," *IEEE Transactions on Communications*, vol. 46, no. 3, pp. 367–371, 1998.

[6] 3rd Generation Partnership Project, "Spatial Channel Model for MIMO Simulations,," 3GPP Technical Specification Group Radio Access Network Tech. Rep. 3GPP TR 25.996 v8.0.0, 2008, http://www.3gpp.org/.

[7] P. Kyösti, J. Meinilä, L. Hentilä et al., "Winner II Channel Models," Tech. Rep. D1.1.2 v1.2, IST-WINNER, 2008, http://www.ist-winner.org/.

[8] L. M. Correia, *Mobile Broadband Multimedia Networks—Techniques, Models, and Tools for 4G*, Elsevier, 1st edition, 2006.

[9] N. Czink, *The random-cluster model—a stochastic MIMO channel model for broadband wireless communication systems of the 3rd generation and beyond*, Ph.D. dissertation, Technische Universität Wien, Forschungszentrum Telekommunikation Wien, Wien, Austria, 2007.

[10] A. J. Levy, "Fine structures of the urban mobile propagation channel," in *Proceedings of COMMSPHERE*, pp. 5.1.1–5.1.6, Herzliya, Ill, USA, 1991.

[11] V. I. Vasylyshyn, "Closed-form DOA estimation with multiscale unitary ESPRIT algorithm," in *Proceedings of the 1st European Radar Conference (EuRAD '04)*, pp. 317–320, October 2004.

[12] W. J. Vogel, H. Ling, and G. W. Torrence, "Fluorescent light interaction with personal communication signals," *IEEE Transactions on Communications*, vol. 43, no. 2, pp. 194–197, 1995.

[13] M. Haardt, *Efficient one-, two-, and multidimensional high-resolution array signal processing*, Ph.D. dissertation, Technische Universität München, Shaker, Aachen, Germany, 1996.

[14] M. Landmann and R. S. Thoma, "Common pitfalls in multidimensional high resolution channel parameter estimation," in *Proceedings of the IEEE 13th Digital Signal Processing Workshop and 5th IEEE Signal Processing Education Workshop (DSP/SPE '09)*, pp. 314–319, Marco Island, Fla, USA, 2009.

[15] J. Fuhl, J. P. Rossi, and E. Bonek, "High-resolution 3-d direction-of-arrival determination for urban mobile radio," *IEEE Transactions on Antennas and Propagation*, vol. 45, no. 4, pp. 672–682, 1997.

[16] M. Haardt and J. A. Nossek, "Simultaneous schur decomposition of several nonsymmetric matrices to achieve automatic pairing in multidimensional harmonic retrieval problems," *IEEE Transactions on Signal Processing*, vol. 46, no. 1, pp. 161–169, 1998.

[17] T. J. Shan, M. Wax, and T. Kailath, "On spatial smoothing for direction-of-arrival estimation of coherent signals," *IEEE Transactions on Acoustics, Speech, and Signal Processing*, vol. 33, no. 4, pp. 806–811, 1985.

[18] X. Li and K. Pahlavan, "Super-resolution TOA estimation with diversity for indoor geolocation," *IEEE Transactions on Wireless Communications*, vol. 3, no. 1, pp. 224–234, 2004.

[19] F. Quitin, C. Oestges, F. Horlin, and P. De Doncker, "Cluster parametrisation for indoor polarized MIMO channels," in *Proceedings of the 8th Management Committee Meeting (COST '09)*, Valencia, Spain, 2009.

[20] N. Czink, P. Cera, J. Salo, E. Bonek, J. P. Nuutinen, and J. Ylitalo, "A framework for automatic clustering of parametric MIMO channel data including path powers," in *Proceedings of the IEEE 64th Vehicular Technology Conference (VTC '06)*, pp. 114–118, Montréal, Canada, September 2006.

[21] N. Czink, P. Cera, J. Salo, E. Bonek, J. P. Nuutinen, and J. Ylitalo, "Improving clustering performance using multipath component distance," *Electronics Letters*, vol. 42, no. 1, pp. 33–34, 2006.

[22] D. J. Kim, Y. W. Park, and D. J. Park, "A novel validity index for determination of the optimal number of clusters," *IEICE Transactions on Information and Systems*, vol. 84, no. 2, pp. 281–285, 2001.

[23] L. Materum, J. I. Takada, I. Ida, and Y. Oishi, "Mobile station spatio-temporal multipath clustering of an estimated wideband MIMO double-directional channel of a small urban 4.5GHz macrocell," *EURASIP Journal on Wireless Communications and Networking*, vol. 2009, Article ID 804021, 16 pages, 2009.

[24] N. Czink, X. Yin, H. Özcelik, M. Herdin, E. Bonek, and B. H. Fleury, "Cluster characteristics in a MIMO indoor propagation environment," *IEEE Transactions on Wireless Communications*, vol. 6, no. 4, pp. 1465–1474, 2007.

[25] J. Poutanen, K. Haneda, J. Salmi, V.-M. Kolmonen, F. Tufvesson, and P. Vainikainen, "Analysis of radio wave scattering processes for indoor MIMO channel models," in *Proceedings of the 8th Management Committee Meeting (COST '09)*, Valencia, Spain, 2009.

[26] M. Steinbauer, A. F. Molisch, and E. Bonek, "The double-directional radio channel," *IEEE Antennas and Propagation Magazine*, vol. 43, no. 4, pp. 51–63, 2001.

[27] A. Nasr, M. Lienard, and P. Degauque, "Extraction of cluster parameters from a block-diagonal form of the channel matrix," in *Proceedings of the 4th Management Committee Meeting (COST '08)*, Wroclaw, Poland, 2008.

[28] E. Tanghe, W. Joseph, M. Lienard et al., "Clustering of channel parameters by block diagonal matrix decomposition," in *Proceedings of the 7th Management Committee Meeting (COST '09)*, Braunschweig, Germany, 2009.

[29] J. L. Myers and A. D. Well, *Research Design and Statistical Analysis*, Lawrence Erlbaum, 2nd edition, 2002.

[30] A. A. M. Saleh and R. A. Valenzuela, "A statistical model for indoor multipath propagation," *IEEE Journal on Selected Areas in Communications*, vol. 5, no. 2, pp. 128–137, 1987.

[31] K. V. Mardia and P. E. Jupp, *Directional Statistics*, John Wiley & Sons, New York, NY, USA, 2000.

[32] Q. Spencer, M. Rice, B. Jeffs, and M. Jensen, "Statistical model for angle of arrival in indoor multipath propagation," in *Proceedings of the 47th IEEE Vehicular Technology Conference*, pp. 1415–1419, May 1997.

[33] A. Abdi, J. A. Barger, and M. Kaveh, "A parametric model for the distribution of the angle of arrival and the associated correlation function and power spectrum at the mobile

station," *IEEE Transactions on Vehicular Technology*, vol. 51, no. 3, pp. 425–434, 2002.

[34] T. W. Anderson and D. A. Darling, "Asymptotic theory of certain "goodness of fit" criteria based on stochastic processes," *Annals of Mathematical Statistics*, vol. 23, no. 2, pp. 193–212, 1952.

[35] S. R. Saunders, *Antennas and Propagation for Wireless Communication Systems*, John Wiley & Sons, New York, NY, USA, 1999.

[36] A. F. Molisch, J. R. Foerster, and M. Pendergrass, "Channel models for ultrawideband personal area networks," *IEEE Wireless Communications*, vol. 10, no. 6, pp. 14–21, 2003.

[37] S. S. Shapiro and M. B. Wilk, "An analysis of variance test for normality (complete samples)," *Biometrika*, vol. 52, no. 3-4, pp. 591–611, 1965.

[38] N. Henze and B. Zirkler, "A class of invariant consistent tests for multivariate normality," *Communications in Statistics*, vol. 19, no. 10, pp. 3595–3617, 1990.

[39] N. Czink, E. Bonek, L. Hentilä, P. Kyösti, J.-P. Nuutinen, and J. Ylitalo, "The interdependence of cluster parameters in mimo channel modeling," in *Proceedings of the 1st European Conference on Antennas and Propagation (EuCAP '06)*, pp. 1–6, Nice, France, 2006.

[40] E. Batschelet, *Circular Statistics for Biology*, Academic Press, 1981.

[41] P. Pagani and P. Pajusco, "Experimental analysis of the ultra wideband propagation channel over the 3.1 GHz-10.6 GHz frequency band," in *Proceedings of the IEEE International Symposium on Personal, Indoor, and Mobile Radio Communications*, pp. 1–5, Helsinki, Finland, 2006.

[42] I. Marinović, I. Zanchi, and Z. Blažević, "Estimation of channel parameters for "saleh-valenzuela" model simulation," in *Proceedings of the International Conference on Applied Electromagnetics and Communications*, pp. 1–4, Dubrovnik, Croatia, 2005.

[43] M. H. Kutner, C. J. Nachtsheim, J. Neter, and W. Li, *Applied Linear Statistical Models*, McGraw-Hill/Irwin, 5th edition, 2005.

[44] X. Zhao, J. Kivinen, P. Vainikainen, and K. Skog, "Propagation characteristics for wideband outdoor mobile communications at 5.3 Ghz," *IEEE Journal on Selected Areas in Communications*, vol. 20, no. 3, pp. 507–514, 2002.